Nanoscale Advances

ROYAL SOCIETY OF CHEMISTRY

PAPER

View Article Online
View Journal

Cite this: DOI: 10.1039/d5na01044f

Fast and cost-effective fabrication of biocompatible polymer nanostructures *via* sublimation-assisted method for drug delivery applications

Gabriella Siani,[ab] Fabrizio Masciulli,[c] Erik Betz-Güttner,[†c] Samanta Moffa,[a] Serena Pilato[ab] and Alessandro Fraleoni-Morgera[*c]

The development of efficient and cost-effective methods to fabricate biocompatible polymer nanostructures is essential for advancing controlled drug delivery systems. In this study, we introduce a rapid and versatile sublimation-assisted method, termed ASB-SANS (Auxiliary Solvent-Based Sublimation-Aided NanoStructuring), for directly forming nanostructures of poly-L-lactic acid (PLLA) and poly(lactic-*co*-glycolic acid) (PLGA) on glass and Si/SiO_x substrates. In this approach, chloroform was used as the auxiliary solvent and *para*-dichlorobenzene (PDCB) as the sublimating agent. Varying the polymer/PDCB ratios systematically from 1 : 50 to 1 : 400 it was possible to control the topology of the resulting nanostructures. Distinct self-assembly behaviours were found between PLLA, which formed elongated nanofibers, and PLGA, which generated highly ordered micro/nanodots arrays. Notably, when loaded with the model drug thionine, ASB-SANS-generated PLGA nanostructures exhibited a significantly suppressed initial burst release (around 60%) compared to the non-nanostructured film, indicating enhanced control over drug release kinetics. This study highlights the potential of ASB-SANS as a powerful method for producing functional polymer nanostructures, offering new opportunities for biomedical applications, particularly in controlled drug delivery systems.

Received 9th November 2025
Accepted 8th April 2026

DOI: 10.1039/d5na01044f

rsc.li/nanoscale-advances

1. Introduction

Nanofibers are ultrafine fibers with diameters typically ranging from a few nanometers to several hundred nanometers, usually below one micrometer.[1] Depending on the source material, nanofibers can be classified as natural (*e.g.*, collagen, cellulose, chitosan) or synthetic (*e.g.*, polycaprolactone, polylactic acid, poly(lactic-*co*-glycolic) acid). Their unique physicochemical properties, such as high surface area-to-volume ratio or tunable porosity have made them attractive candidates for a wide array of applications, including drug delivery, tissue engineering, filtration, and energy storage.[2–5]

In tissue engineering, nanofiber-based scaffolds closely mimic the architecture and function of the extracellular matrix (ECM), providing a favourable environment for cell adhesion, proliferation, and tissue regeneration. To this end they have been successfully applied in skin, bone, cartilage, vascular and nerve tissue repair.[6–10]

In drug delivery, nanofibers serve as carriers able to modulate the release kinetics of therapeutic agents, supporting sustained or stimuli-responsive administration.[11–13] The polymeric composition of these nanostructures, both natural and synthetic, plays a critical role in tuning properties such as mechanical strength, degradation rate and drug loading efficiency.[14–16] Nanofiber-based delivery systems have gained increasing attention for their potential to overcome the limitations of conventional formulations, including rapid degradation, poor solubility and systemic toxicity.[17,18] Indeed, recent studies have highlighted that both nanoscale structuring and molecular design strategies can serve as powerful tools to regulate transport, release dynamics, and functional performance in advanced soft material systems, complementing conventional chemical and material selection approaches.[19–22]

For ensuring effectiveness in drug delivery, polymers must satisfy stringent criteria such as biocompatibility, biodegradability, non-immunogenicity and controlled degradation rates tailored to therapeutic needs, ensuring optimal therapeutic effects. In this frame, poly(L-lactic acid) (PLLA), poly(glycolic acid) (PGA), and their copolymer poly(lactic-*co*-glycolic acid) (PLGA) are among the most widely utilized materials for drug

[a]*Dipartimento di Farmacia, Università "G. d'Annunzio" Chieti-Pescara, Via dei Vestini 31, 66013 Chieti, Italy*

[b]*UdA-TechLab, Research Center, Università degli Studi Gabriele d'Annunzio Chieti-Pescara, Via dei Vestini 31, 66100 Chieti, Italy*

[c]*Dipartimento di Ingegneria e Geologia, Università "G. d'Annunzio" Chieti-Pescara, Viale Pindaro 42, 65100 Pescara, Italy. E-mail: alessandro.fraleoni@unich.it*

† Present address: Debye Institute for Nanomaterials Science, Utrecht University, Heidelberglaan 8, 3584 CS Utrecht, The Netherlands.

delivery systems, due to their excellent biocompatibility, biodegradability and mechanical stability.[23–25] These polymers are readily absorbable, and they are naturally degraded *via* enzymatic and non-enzymatic pathways into non-toxic byproducts, such as lactic and glycolic acid, which are readily metabolized.

In particular, the degradation rate of PLGA can be tuned by adjusting the lactic-to-glycolic acid ratio, allowing precise control over drug release profiles.[26] In addition, the large surface area of nanofibers enables high loading efficiency for both hydrophilic and hydrophobic drugs, facilitating sustained release and enhancing patient compliance. PLLA and PLGA nanofibers have been hence extensively investigated for the delivery of antibiotics, anticancer agents and other bioactive molecules such as growth factors or nucleic acids, opening new possibilities for regenerative medicine and targeted therapies.[27–30] Among the fabrication techniques available for fabricating nanofibers, electrospinning is the most widely used one, allowing continuous production with controlled fiber diameter, porosity and surface morphology.[31,32] However, electrospinning has several drawbacks, including the requirement for high-voltage equipment, extremely low nanofibers production rates – a few mm^3 per hour, and the need for controlled environments, which limit scalability and increase production costs.[33,34]

Recently, an alternative nanostructuring strategy, named Auxiliary Solvent-Based Sublimation-Aided Nanostructuring (ASB-SANS), has emerged as a promising platform for the fabrication of hierarchically organized nanofibers and aligned nanodots.[35,36] This innovative, self-assembly-based method relies on a ternary liquid solution composed by an auxiliary solvent (AS), a sublimating substance (SS), and a target material (TM), typically the polymer to be nanostructured. As a liquid solution, the mixture can be easily and rapidly manipulated and deposed on various surfaces, even at room temperature and with no specific equipment, also taking advantage from extremely common and simple glassware. The TM is selected for its solubility in both AS and SS and is used in small amounts within the mixture (usually between 0.1% and 5% in weight with respect to the SS). The SS must satisfy several criteria: (i) solubility in the AS, (ii) ability to fully dissolve the TM also in the solid phase, (iii) sublimability at a temperature lower than the evaporation temperature of the AS, (iv) crystallizability (if one wants to create ordered nanostructures out of the TM).

Upon deposition of the ternary solution onto a substrate, the evaporation of the AS triggers the crystallization of the SS, which forms a solid, crystalline solution incorporating the TM as a solute. As the SS gradually sublimates, the embedded TM migrates within the SS matrix until it reaches the boundaries of SS crystallites, where it precipitates to form well-organized nanofibers or nanodots, depending on the relative concentrations of the three components of the mixture.[36] Notably, the SS acts as a physical template, driving the spatial organization of the TM, and at the end of the process it simply disappears, avoiding several common problems of template-based nanofabrication, like the need for further processing steps to eliminate the template.

ASB-SANS offers further several key advantages. First of all, it is extremely fast, enabling in some cases nanostructure formation in minutes; even for particularly complex cases, the nanostructure formation is rarely longer than a few hours. It is definitely cost-effective, requiring only common glassware and plasticware, reagents and solvents and easily available deposition tools and methods (no need for clean rooms, high vacuum equipment, glove boxes or the like). The size and type of the obtained nanostructures can be controlled by the simple tuning of the relative concentration of the three components of the mixture.[36] Moreover, it can produce nanostructures over several cm^2 with one single fabrication step, and it is effective over most of the commonly used substrates (glass, flexible polyimide, silicon/silicon oxide chips, gold-coated substrates), even when discontinuities between different materials are present.[35–39] Finally, it is highly versatile, as it has been demonstrated effective with a wide variety of polymers and nanomaterials, including polymethylmetacrylate (PMMA),[35] PLA[37] or PLGA,[38] semiconducting polymers like poly(3-hexylthiophene) (P3HT)[39,40] and carbon nanotubes.[35]

Thanks to these characteristics, the method has been applied in various fields such as gas sensing,[39] tissue engineering,[37] and direct lithographic masking.[36] Nonetheless, it remains underutilized in biomedical drug delivery research, despite its significant potential for scalable and affordable nanostructure fabrication.

In this work, we hence explore the ASB-SANS technique to fabricate nanostructures of PLLA and PLGA and to assess their applicability as drug delivery platforms. To this aim thionine, a model hydrophilic compound, was incorporated into PLGA nanostructures in the same nanofabrication step ("one pot dye incorporation" into the nanostructures), and its release profile was followed and compared to that of non-nanostructured films of the same polymeric material. Our results demonstrate the efficacy and convenience of ASB-SANS as a low-cost, fast, and simple method for producing biocompatible nanostructures with controlled drug release properties, paving the way for future biomedical applications.

2. Experimental

2.1 Chemicals and materials

Poly(L-lactic acid) (PLLA, MW 258 700), poly(lactic-*co*-glycolic acid) (PLGA, 50 : 50, MW 38 000–54 000), chloroform ($CHCl_3$), *para*-dichlorobenzene (PDCB), thionine acetate salt, and all salts used for the buffer preparation were purchased from Sigma-Aldrich and used without further purification. All reagents were of analytical grade. Water was doubly distilled, deionized and HPLC grade.

p-Doped Si/SiO_x wafers (100) were purchased from ITME, Warsaw, Poland.

2.2 Instruments

Optical micrographs were acquired using a Nikon Eclipse i50 (Tokio, Japan) microscope equipped with a Nikon Digital Sight DS-2Mv imaging system.

Scanning electron microscopy (SEM) analysis was performed using a Carl Zeiss Supra 40 Scanning Electron Microscope, Oberkochen, Germany.

UV-vis absorption spectra were recorded using a PerkinElmer UV/vis Spectrometer Lambda Bio 20.

2.3 Substrate preparation

p-Doped Si/SiO_x substrates were used to facilitate optimal SEM characterization of the nanostructures. The substrates were cleaned with acetone and isopropyl alcohol, then dried under a stream of nitrogen gas. Substrate cleanliness was found to be critical for achieving well-organized nanostructures as insufficient cleaning reduced the wettability of the silicon surface by the ternary solution, resulting in the formation of amorphous, poorly defined polymer aggregates.

2.4 Fabrication of nanostructures *via* the ASB-SANS method

To obtain polymeric nanostructures *via* the ABS-SANS technique, ternary solutions were prepared using PLLA or PLGA as the target material (TM), PDCB as the sublimating substance (SS), and $CHCl_3$ as the auxiliary solvent (AS). A stock solution was prepared by dissolving 1 mg of the chosen polymer in 1 mL of $CHCl_3$ and stirring the mixture for 8 hours to ensure complete polymer dissolution. The SS concentration was varied to obtain different polymer/PDCB w/w ratios (for PLLA: 1 : 50, 1 : 100, 1 : 200, 1 : 400; for PLGA: 1 : 50). The resulting homogeneous ternary solutions were drop-cast onto substrates. After $CHCl_3$ evaporation, PDCB gradually sublimated, forming a thin solid, crystalline layer (estimated thickness around 300 μm) promoting the self-assembly of polymeric nanostructures. During the process, the temperature was maintained at 25(±0.2) °C, using a temperature-controlled plate, well below the melting point of PDCB (53 °C). After approximately 1 hour from the deposition of the ternary solution, the samples underwent a vacuum treatment using a standard double-diaphragm pump for an additional hour to ensure complete removal of residual PDCB.

Control, non-nanostructured polymer films were prepared by drop casting a polymer solution at the same TM/AS ratio (*i.e.*, 1 mg of polymer in 1 mL of $CHCl_3$) in the absence of PDCB.

2.5 Release experiments

Thionine was added to the ternary solution used to obtain PLGA nanostructures and to the control PLGA solution used to obtain non-nanostructured films at a final concentration of 10^{-3} M. The resulting films and nanostructures were washed with 2.5 mL of physiological solution to remove any dye particles possibly adsorbed on the outer surface. Two types of experiments were conducted to quantify the thionine release from nanostructured and non-nanostructured PLGA. In both cases, three samples were placed in 60 mm diameter glass Petri dishes and immersed in 8 mL of phosphate-buffered saline (PBS). Temperature was maintained at 37 °C using a thermostated convection oven equipped with a thermocouple. To prevent excessive drying of the PBS, beakers containing distilled water were placed inside the oven, and the PBS solution was pre-heated and stored in a closed container within the same oven.

In the first experimental setup, 2.5 mL of the solution were collected at predefined time intervals for UV-vis analysis, to monitoring thionine release at its maximum absorbance (598 nm (ref. 41)). After each sampling, an equal volume of fresh PBS was added. Sampling intervals ranged from 1 to 40 minutes. In the second experimental setup, a more exhaustive protocol was followed. Each sample was immersed in 7 mL of PBS, and the entire volume was removed at each timepoint. The Petri dishes and samples were then rinsed and re-immersed in fresh buffer. This approach aimed to eliminate any cumulative concentration effects and allow accurate assessment of time-dependent release dynamics. However, the results obtained from both experimental setups were largely superimposable, indicating that the release kinetics were not significantly affected by the sampling method and validating the robustness of the observed release trends.

2.6 Statistical analysis

Statistical analysis of kinetic data was performed using GraphPad Prism 5. All results are based on at least three independent experiments and are expressed as mean ± standard deviation (SD). Statistical differences between group means were assessed using Student's *t*-test (two groups). A p-value <0.05 was considered statistically significant. The AFM image analysis has been conducted using ImageJ 1.54G for MacOs.

3. Results and discussion

3.1 Preparation of polymer nanostructures by ASB-SANS method

PLLA and PLGA were selected due to their known biocompatibility and bioresorbability. Notably, PLGA offers tunable degradation rates depending on the ratio of its constituent monomers. The ability of both polymers to self-assemble into nanostructures using the ASB-SANS method has been previously reported.[37,38]

The ASB-SANS method relies on a three-components solution, in which the material to be nanostructured (Target Material, TM, usually a polymer) is dissolved in a mixture of a liquid solvent (Auxiliary Solvent, AS) and a solid substance capable of sublimation (Sublimating Substance, SS). Briefly, the choice of the three components is made on the basis of the TM selected for creating the nanostructures. Upon this selection, the AS and SS are chosen among the materials able to both dissolve the selected TM and to be reciprocally mixable, in order to obtain a homogeneous ternary solution after the mixing. Moreover, further criteria of choice of the AS and SS include that the AS must have a low boiling point, so to allow it to evaporate much before the SS starts to appreciably sublimate. A further requirement needed when the formation of nanofibers, or of aligned nanostructures, out of the selected TM is desired, is that the SS must be able to form crystal with a tendentially linear habit, as this compound provides a template for the ordered self-assembly of the TM during the sublimation phase. In this

case the concentration of the TM with respect to the SS should be kept at 1 : 100 w/w or less, otherwise the TM will tend to impede the crystallization of the SS.

After these criteria are fulfilled, the formation of the nanopatterns occurs as follows: (i) the TM/AS/SS ternary solution is deposed onto the chosen substrate; (ii) the AS evaporates, leaving a crystalline solid SS/TM solution on the substrate; (iii) the SS sublimated away, leaving on the substrate the TM organized in the desired nanopatterns. A more detailed description of this procedure is provided in previous work.[35,36]

Para-dichlorobenzene (PDCB) was selected as SS for its ability to dissolve a variety of organic materials, including PLA and PLGA, its tendency to form needle-like crystals, and its full solubility in $CHCl_3$. $CHCl_3$ was chosen as the AS due to its low boiling point (about 60 °C), which makes for its complete evaporation much before the PDCB, at atmospheric pressure, starts to meaningfully sublimate. In particular, highly ordered and hierarchically organized long-range nanofibers have been fabricated from PLLA. These structures supported the growth of several cell lines, confirming successful cell culture and demonstrating an excellent biocompatibility of ASB-SANS-generated structures.[37] Similarly, the same technique enabled the fabrication of well-aligned PLGA nanofibers over remarkably large areas, spanning several cm^2, with individual fibers extending several centimeters in length. These nanofibers displayed strong adhesion to both homogeneous and heterogeneous substrates. The auxiliary solvent $CHCl_3$ facilitated the rapid formation of a solid PDCB/polymer film within minutes of deposition, due to its relatively low boiling point (~62 °C). Infrared spectroscopy carried out on the realized samples confirmed the absence of residual chloroform in PLLA nanostructures after the ASB-SANS process, in line with previous studies.[37]

Given that the TM/SS ratio has been shown to influence the topology of nanostructured patterns in PMMA-based ternary solutions,[36] four PLLA/PDCB formulations with ratios ranging from 1 : 50 to 1 : 400 were prepared and deposited onto Si/SiO_x substrates, with the aim of identifying the optimal operative conditions for PLLA nanofiber formation (a few preliminary experiments were carried out using standard and less expensive microscope glass slides, leading to the same results hereafter described, despite the much rougher surface. This is in line with already reported results, which showed a high robustness of the ASB-SANS method with respect to the used type of substrate[38]). The resulting morphologies were initially assessed *via* optical microscopy. Representative micrographs are shown in Fig. 1.

As is visible, PLLA nanostructures uniformly covered large surface areas (in the cm^2 range) with consistent density and homogeneity, although a nanometrically precise repetition of the patterns is not always achieved, due to the manual conditions of the ternary solution deposition, also carried out in open air, hence subjected to randomly oriented air flows. Despite of these apparently sub-optimal conditions, from Fig. 1 it is possible to appreciate that decreasing the PLLA/PDCB ratio led in general to a progressive rarefaction of the fibers and to an increase in inter-fiber spacing, as reported in previous studies.[35,36] This is due to the higher amount of PDCB, acting as the crystallizing template, which in turn allows the polymer chains to diffuse for longer distances before precipitating upon

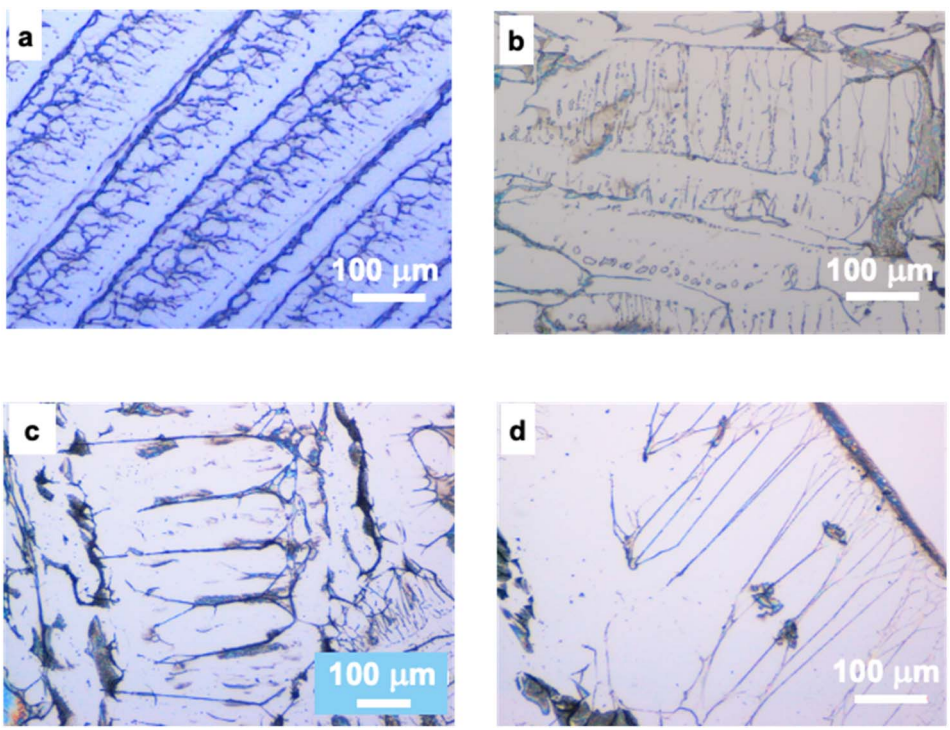

Fig. 1 Optical microscope images of PLLA nanostructures obtained at room temperature upon chloroform evaporation and PDCB sublimation at PLLA/PDCB ratio (a) 1 : 50, (b) 1 : 100, (c) 1 : 200, (d) 1 : 400.

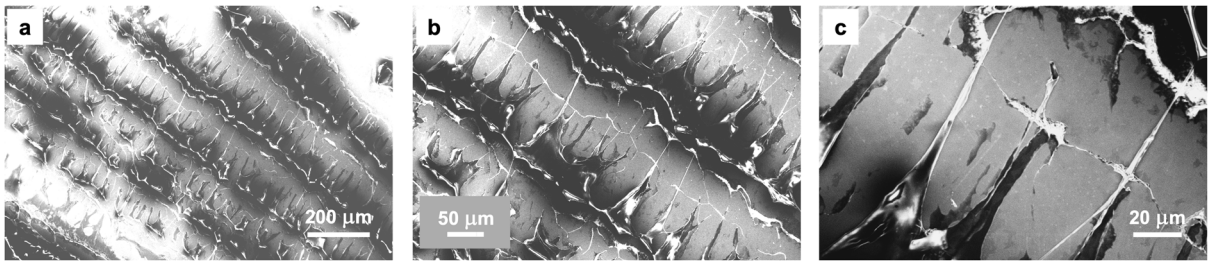

Fig. 2 SEM images of PLLA nanostructures, obtained from the ASB-SANS solution with a TM/SS ratio of 1 : 50 deposited on Si/SiO_x chips, at different magnifications. From panel (a) it is possible to appreciate that the patterns are developed over a pretty large surface, more than a mm^2; panels (b) and (c) are progressively higher magnifications, which show a reasonable regularity of the distribution of the patterns.

complete PDCB sublimation. The observed trend is consistent with previous findings: as in any ternary solution, the higher amounts of PDCB reduced the relative concentrations of the other two components, *i.e.* the polymer (PLLA) and the auxiliary solvent ($CHCl_3$), promoting the formation of larger PDCB crystallites.[36] As a consequence, longer sublimation times in presence of small amounts of PLLA resulted in more fragmented and irregular polymer patterns.

Based on these results, a PLLA/PDCB ratio of 1 : 50 was selected for subsequent experiments, due to an acceptable balance between large surface extended patterns, necessary for allowing optimal dye release, and nanofiber continuity, essential for reliable estimation of release kinetics and rates.

To further elucidate the morphological features of the nanostructures, SEM analysis was conducted on the chosen 1 : 50 PLLA/PDCB samples.

The SEM images (Fig. 2) revealed that the developed nanostructures are characterized by a hierarchical organization. Primary larger microfibers (1–2 μm as lateral width) are continuous, wavy and relatively irregular but well aligned with each other, and extend for several millimeters along the sample (Fig. 1a and 2a). Secondary fibers, much smaller (with width between 1 μm and a few hundreds nm) and more straight, are developed orthogonally to the primary ones. This topology reflects the intrinsic crystalline habit of PDCB and aligns with previous observations made for different polymer systems using PDCB as the sublimating substance.[35–37]

PLGA-based nanostructures were obtained from ternary solutions with PLGA/PDCB ratios of 1 : 50. Optical microscopy revealed a markedly different outcome of the ASB-SANS procedure for PLGA compared to PLLA. Indeed, PLGA formed aligned rows of dots having diameters in the range of a few microns/several hundreds of nanometers, instead of nanofibers, as shown in Fig. 3.

The formation of the observed aligned globular structures from PLGA, rather different from the continuous nanofibers formed by PLA, can be explained in light of a few characteristic phenomena typical of polymer chains in diluted solutions and confined environments. In fact, it is known that globular polymeric structures are formed in liquid solutions when non-solvent is added to the system (so called "coil-to-globule transition",[42,43] and that solid substrates can enhance this formation *via* surface effects[44]). In our case the low concentrations of polymer within the sublimating substance result in a diluted solid solution. The laboratory atmosphere (normal air) works as a non-solvent for the polymer, which upon progressive sublimation of PDCB loses its solid-state solvent, leading the system towards the precipitation of PLGA on the underlying substrate as globules, aligned along the edges of the previously developed SS/TM crystallites (as described more in detail in ref. 36). The fact that PLGA tends to form nanodots rather than the nanofibers created by PLA is attributed to the higher polarity of PLGA with respect to PLA. As PDCB is an apolar molecule, PLGA is less soluble in it than PLA, leading to a faster precipitation and to the observed formation of the coil-to-globule transition. This explanation is supported, besides the clear chemical differences in the structures of PLA and PLGA, also by the available literature for the Hansen solubility parameter for the three considered compounds (Table 1). The Hansen solubility value is a widely recognized empirical parameter able to provide useful indications about the solubility of materials. It is based on concepts previously developed by Hildebrand, for which the process of solubilization of a compound in a solvent implies the complete loss of its cohesive energy δ, *i.e.* the breakage of its intermolecular bonds.[45] As this concept was proven useful but not always applicable to hydrogen-bonding species, Hansen developed it into a more general model accounting also for hydrogen bond-capable species, based upon three parameters δ_D, δ_P and δ_H, assigned to the components of cohesive energy attributable to forces of dispersion, polarization and hydrogen bonding, respectively.[46] Briefly, in this frame the considered solubility parameters are viewed as components of a three-dimensional vector which defines a solubility space; the smaller the value of R_a, a calculated "distance" according to eqn (1) between the Hansen parameters of the solute and those of the solvent, the easier the solubility of the considered compound in the considered solvent.

$$R_a = [4(\delta_{D1} - \delta_{D2})^2 + (\delta_{P1} - \delta_{P2})^2 + (\delta_{H1} - \delta_{H2})^2]^{0.5} \quad (1)$$

Table 1 shows the Hansen parameters for PDCB, PLA and PLGA (lactic to glycolic ratio 50 : 50) as recovered from available literature.[46–50]

As is visible, the Hansen solubility parameter R_a for the couple PDCB/PLA is always appreciably smaller than the

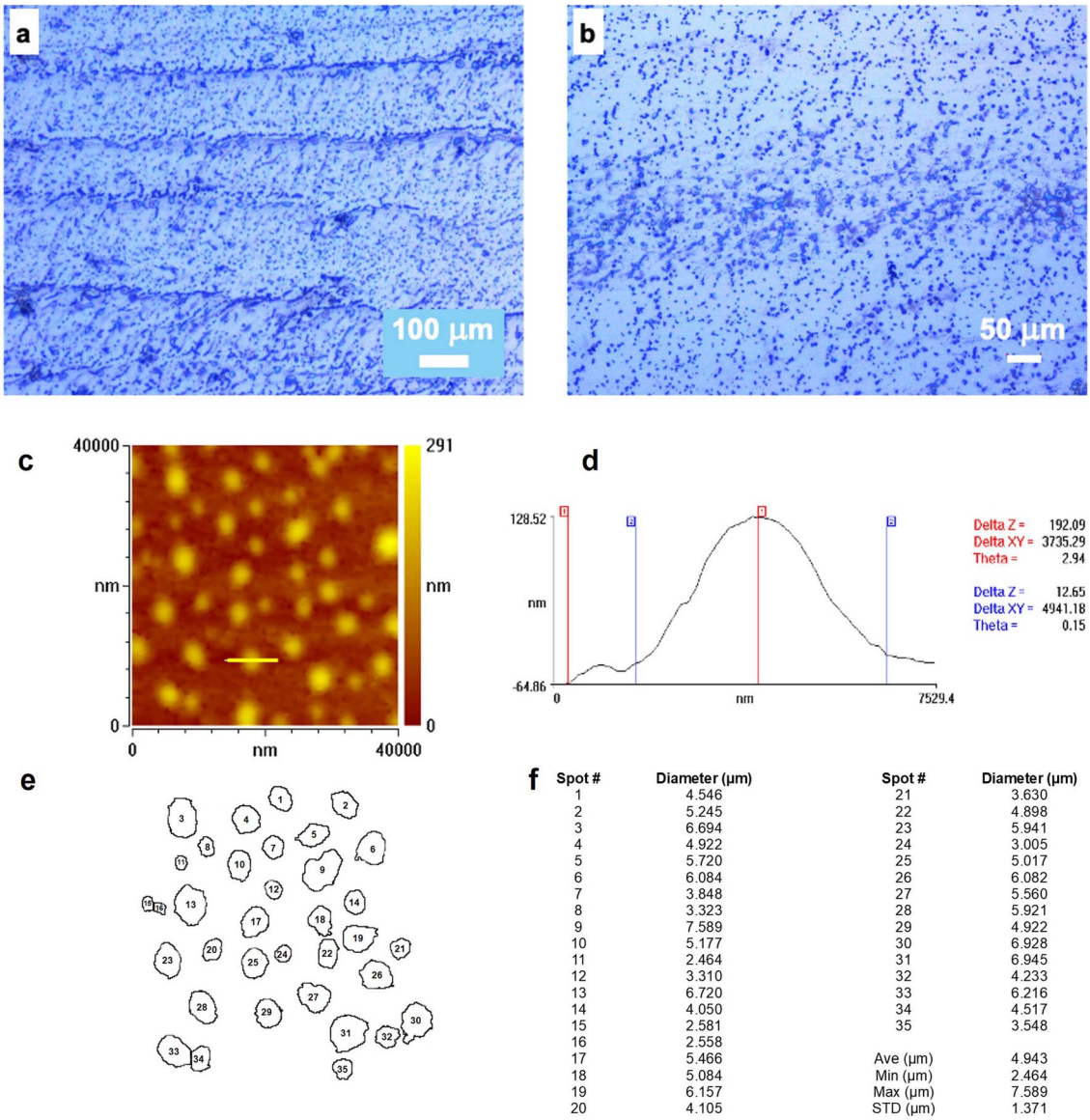

Spot #	Diameter (µm)	Spot #	Diameter (µm)
1	4.546	21	3.630
2	5.245	22	4.898
3	6.694	23	5.941
4	4.922	24	3.005
5	5.720	25	5.017
6	6.084	26	6.082
7	3.848	27	5.560
8	3.323	28	5.921
9	7.589	29	4.922
10	5.177	30	6.928
11	2.464	31	6.945
12	3.310	32	4.233
13	6.720	33	6.216
14	4.050	34	4.517
15	2.581	35	3.548
16	2.558		
17	5.466	Ave (µm)	4.943
18	5.084	Min (µm)	2.464
19	6.157	Max (µm)	7.589
20	4.105	STD (µm)	1.371

Fig. 3 (a) and (b) Microscope images of PLGA nanostructures obtained at room temperature upon chloroform evaporation and PDCB sublimation at PLGA/PDCB ratio of 1 : 50 on Si/SiO_x chips, at different magnifications; (c) and (d) AFM image of a selected zone of the same sample and height profile of the nanodot highlighted in panel (c) with a yellow line; (e) outlined version of (c); (f) results of data analysis of (c).

analogous R_a for the couple PDCB/PLGA (50 : 50), independently from the considered PDCB/polymer couples (the absolute values of the Hansen parameters are known to be subject to variability upon different methods of measurement/calculation, molecular weight and/or defectivity degree in case of polymers and other experimental conditions), strongly suggesting that PLGA is lesser soluble in PDCB than PLA.

Despite of the evidently different morphology between PLA and PLGA nanopatterns, the PLGA micro/nanodots, with typical diameters around a few units of microns and heights of a couple

Table 1 Hansen solubility parameters collected from available literature for PDCB, PLA and PLGA (LA : GA 50 : 50)

Compound	δD ($MPa^{0.5}$)	δP ($MPa^{0.5}$)	δH ($MPa^{0.5}$)	R_a PDCB-1/polymer ($MPa^{0.5}$)	R_a PDCB-2/polymer ($MPa^{0.5}$)
PDCB-1 (ref. 46 and p. 125) (solvent)	19.7	5.6	2.7		
PDCB-2 (ref. 47) (solvent)	18.8	4.61	7.61		
PLA-1 (ref. 48) (solute)	18.6	9.9	6	5.85	6.66
PLA-2 (ref. 49) (solute)	18.88	4.61	7.61	5.27	9.50
$PLGA^{50}$ (LA : GA 50 : 50) (solute)	17.4	9.1	10.5	9.71	10.51

hundreds of nm, as measured by AFM (Fig. 3c and d) do align nicely to form main lines (Fig. 3a), while sparse dots (sometimes orthogonally aligned to the main lines) are distributed pretty uniformly between the main lines (Fig. 3b). A typical measurement of well separated nanodots is reported in Fig. 3c–f, showing that the dots have an average diameter of about 4.9 μm (STD of about 1.37 μm) and a height ranging around 0.2 μm, even though higher dots have been found, especially in the denser zones.

3.2 Release experiments

Sustained drug release remains one of the most effective strategies in drug delivery, and as such, has been extensively explored in the literature. Among the many drug delivery systems (DDS), polymer-based nanofibers have attracted growing attention over the past two decades, surpassing even nanoparticles, due to their exceptionally large surface area.[51,52] These structures are widely recognized for enhancing both biodistribution and bioavailability of hydrophilic and lipophilic drugs.[53,54] PLLA and PLGA, due to their biocompatibility and biodegradability, are commonly used for drug encapsulation and have demonstrated high efficacy in this field.[55,56] Electrospinning is one of the most employed techniques for fabricating polymer nanofibers.[57–59] However, fiber formation through electrospinning depends on numerous interrelated parameters, including polymer concentration, solution viscosity, surface tension, conductivity, solvent properties, applied voltage, collector geometry, and the needle-to-collector distance,[60] and a correct balance of these parameters for obtaining the desired outcomes in terms of nanofiber diameters and characteristics is sometimes very difficult. Moreover, the operating conditions (among which the high tension needed for proper working – several kV of potential difference between the needle and the collector or the use of specific fluorinated solvents that become dispersed in the working environment) create some hazard that could be desirable to avoid. In this context, the ASB-SANS technique presents a potentially simpler and more efficient alternative for fabricating polymer nanofibers suitable for drug delivery. Nevertheless, no prior studies have reported the use of ASB-SANS for this specific purpose.

The formation of PLLA nanofibers by ASB-SANS was shown to be rapid and effective, and led to well organized and relatively homogeneous systems. However, while PLLA is fully biocompatible and bioresorbable, its degradation time is considerably longer (several weeks to months) than that of PLGA, which can degrade within hours or days depending on its lactic-to-glycolic acid ratio. For practical reasons, including the need to complete release experiments within a reasonable time frame, PLGA was hence selected as the matrix material.

In fact, PLGA is approved for medical applications due to its non-toxic, biodegradable and biocompatible nature.[61] It degrades *via* hydrolysis into its constituent components, which are further metabolized into harmless byproducts such as water and carbon dioxide, resulting in minimal toxicity. The polymer's degradation rate can be tailored from one week to several months by adjusting its molecular weight and LA/GA ratio (the higher this ratio, the longer the degradation time), enabling sustained drug release.[26] It is hence an ideal polymer for carrying out proof-of-concept studies for controlled release experiments for drug delivery purposes in reasonably shot time spans.

Thionine acetate salt (hereafter referred to as thionine) was selected as a model hydrophilic compound for preliminary drug loading and release experiments. It is an effective cell stain[62,63] and has been proposed as an inhibitor of both BuChE and AChE.[64] Thionine is also advantageous due to its strong absorbance in the UV-vis range (molar extinction coefficient around 54 000 $dm^3\ mol^{-1}\ cm^{-1}$ at 598 nm), facilitating its quantitative detection.[65]

Crucially, as an ionic dye, thionine is insoluble in chloroform and scarcely soluble within the yet polar PLGA, but it is readily soluble in water and PBS. Due to these characteristics, its addition to the ternary mixture PLGA/$CHCl_3$/PDCB resulted in the formation of micronized dye aggregates within the solid polymer matrix, which were visible under optical microscopy. On the other hand, upon immersion in PBS the thionine released from the solid PLGA/thionine nanostructures in the aqueous environment allowed its rapid and quantitative detection *via* UV-vis spectrophotometry. Therefore, despite the observed non optimal incorporation of thionine within the PLGA matrix, we decided to use this latter dye as our model release compound.

To study the release of thionine from PLGA two types of samples were prepared: continuous PLGA films (used as control samples), and ASB-SANS-generated PLGA nanofibers. Both types were loaded with thionine.

PLGA films were fabricated by drop-casting a PLGA/$CHCl_3$/thionine solution onto substrates without PDCB. Initial attempts revealed a pronounced "coffee ring" effect, where the dye and polymer accumulated at the droplet edges upon solvent evaporation (Fig. 4a). To prevent this material accumulation, which could have compromised the release experiments, two approaches were tested. The first one involved adding a small percentage of a high-boiling solvent to the chloroform solution, as it is known that a mixture of high- and low-boiling solvents can mitigate the coffee ring effect.[66] The second approach used a simple mechanical technique, by manually shearing the droplet using a glass slide to uniformly distribute the solute before evaporation completed.

For the first approach, the addition of 5% v/v toluene (b. p. ∼ 111 °C) yielded a relatively uniform dispersion of micronized thionine (approximate grain size of about 10 μm) within the solid film (Fig. 4b). The second approach, *i.e.* spreading the deposited solution with a glass slide used as a spatula, was found to be even more effective, producing films with uniformly distributed dye aggregates of finer size (around a few units of μm, Fig. 4c). This latter sample was hence selected as plain control film (*i.e.*, no nanostructures) to be compared with the behaviour of the ASB-SANS-generated, nanostructured PLGA.

Once the homogeneous films were obtained, tests were conducted to determine the optimal dye concentration and solution volume needed to achieve detectable results *via* UV-vis spectrophotometry. A thionine concentration of 10^{-3} M was

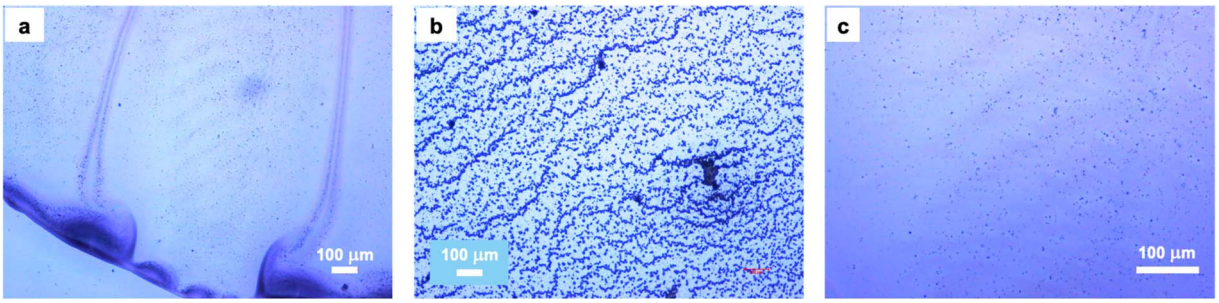

Fig. 4 Microscope images of solid PLGA films obtained by depositing a $CHCl_3$/PLGA/thionine solution onto glass slides. (a) Example of PLGA and thionine accumulation at the PLGA/thionine solid film interface with the glass slide. The dye streaks running from the bottom to the top of the image have been caused by convective phenomena within the droplet, which transported the thionine aggregates along precise lines; (b) thionine aggregates within the solid PLGA film obtained by mixing the $CHCl_3$/PLGA/thionine mixture with toluene; (c) thionine aggregates within the solid PLGA film obtained shearing the $CHCl_3$/PLGA/thionine solution with a plain spatule. All the imaged solid films have been obtained depositing on the glass substrate a $CHCl_3$ (1 mL)/PLGA (1 mg)/thionine (10^{-3} M) solution; only for (b) the mentioned solution has been added by 5% in total ternary solution volume of toluene.

selected, providing absorbance values well within the UV-vis calibration range. This same concentration was applied in the preparation of ASB-SANS nanofibers, enabling direct comparison of the release behaviour between plain and nanostructured films.

Before proceeding with the release tests, all samples were rinsed with 2.5 mL of PBS to remove unincorporated or surface-adsorbed thionine. Release experiments were then conducted at 37 °C to simulate physiological condition.

The normalized thionine release profiles for both sample types are presented in Fig. 5.

To characterize the release behaviour, two different kinetic models were applied to fit the release profiles. The first was a first-order kinetic model based on the general rate expression (eqn (2)):

$$[\text{dye}]_{\text{eq}} - [\text{dye}]_t = Ae^{-t/k_{\text{obs}}} \quad (2)$$

The second was a biphasic kinetic model, which considers two distinct release phases and is described by kinetic eqn (3):

$$[\text{dye}]_{\text{eq}} - [\text{dye}]_t = Ae^{-t/k_1} + Be^{-t/k_2} \quad (3)$$

In these models, $[\text{dye}]_{\text{eq}}$ and $[\text{dye}]_t$ are the total concentrations of thionine released at equilibrium and at time t, respectively; k_{obs} is the first-order kinetic constant, and k_1 and k_2 are the rate constants for the burst and the sustained release step, respectively.

The correlation coefficients (R^2) were calculated to assess the quality of the model fits.

The release kinetics followed a biphasic model, characterized by an initial burst phase followed by a slower, sustained release. Correlation coefficients ($R^2 \geq 0.996$) confirmed excellent model fitting. The corresponding rate constants for both phases, k_1 for the burst release and k_2 for the sustained release, are reported in Table 1. This kinetic modelling effectively captures the heterogeneity of the release process and highlights differences between the two systems.

The proposed release mechanism is illustrated in Fig. 6.

In more detail, in the burst phase the dye is released from the most external layers of the system, while in the swelling phase the polymer macromolecules get hydrated and more mobile, allowing the rest of the dye to be released in the outer environment.

The general degradation behaviour of PLGA is primarily due to bulk erosion. As water enters the polymer, hydrolysis gradually creates pores that grow and coalesce, accelerating dye release. In turn, the initial burst release likely results from these pore formations and surface defects, which allow rapid dye diffusion.[67,68]

The kinetic constant values for the two phases, determined by fitting eqn (2) to the kinetic profiles, are presented in Table 2. They indicate that the sustained release from both the standard film and nanostructured PLGA occurs at nearly the same rate, whereas the initial burst release from the fibers is definitely slower than that from the film, as evidenced by the remarkable difference between k_1 of the plain film with respect to that of the nanostructured PLGA, where the former is about 60% larger than the latter.

The different release behaviour observed in the nanostructured PLGA samples compared to plain films is likely due

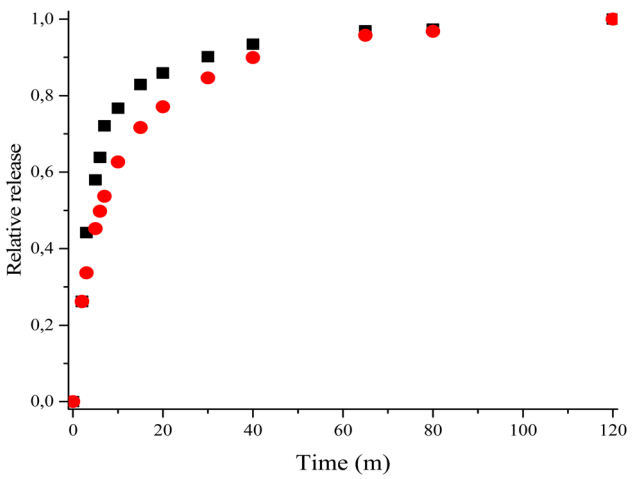

Fig. 5 Normalized kinetic profiles of the spontaneous release of thionine at 25 °C from PLGA film (black line) and PLGA nanostructures (red line).

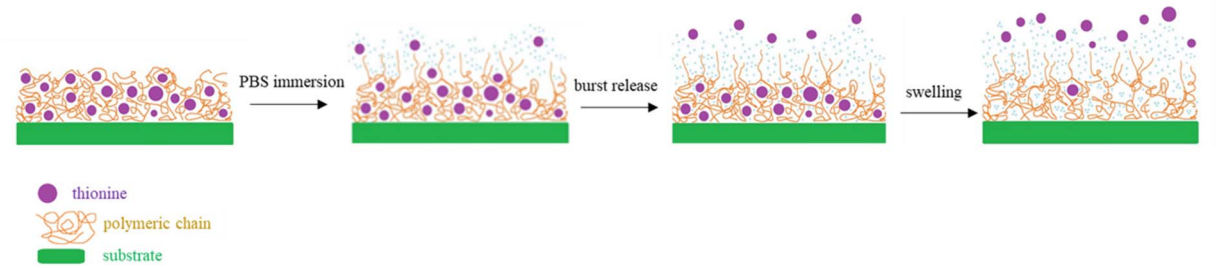

Fig. 6 Hypothesized mechanism for thionine release from PLGA film and nanostructures.

Table 2 Rate constant values for the burst (k_1) and sustained (k_2) release of thionine from the investigated systems. Statistical analysis was performed using Student's *t*-test, confirming that the difference between the k_1 values was statistically significant (p-value < 0.05)

System	k_1 (m^{-1})	k_2 (m^{-1})
PLGA film	0.496 ± 0.131	0.0383 ± 0.0080
PLGA nanostructures	0.207 ± 0.039	0.0358 ± 0.0036

to the higher crystallinity of the dots generated *via* the ASB-SANS method, as previously reported.[36,40] In fact, higher crystallinity leads to denser macromolecular packing, which hinders water penetration, making the processes of both polymer swelling and degradation slower. In the ASB-SANS-produced micro/nanodots, the increased structural compactness reduces early-stage pore formation, with a notable 60% decrease in the burst rate, thus moderating the burst release effect compared to non-structured films. This effect is even more notable when considering the much higher specific surface exposed to the liquid by the nanostructured polymer with respect to that of the plain film. Over time, as the polymer continues to hydrate and degrade and most of the dye has been released, in both systems the overall release rate slows, ultimately reaching similar levels.

As a result, the initial burst release is reduced by ~60% compared to non-structured films, although a residual burst remains, likely due to dye molecules located near the polymer surface or early-stage pore formation, as commonly observed in nanostructured polymer systems.[69–71] Comparative modeling of release kinetics between nanostructured PLGA and non-structured films, as shown in Table 2, highlights that the ASB-SANS nanostructures significantly reduce the initial burst release rate (k_1) while maintaining similar sustained release kinetics (k_2). This quantitative comparison clearly demonstrates the effect of nanostructuring on controlled release behavior and confirms that the ASB-SANS approach effectively modulates the early release phase without compromising long-term sustained release.

4. Conclusions

In this study, we demonstrated the effectiveness of the ASB-SANS technique in rapidly fabricating nanostructured polymer architectures, such as nanofibers and micro/nanodots, under relatively simple and mildly controlled conditions. Remarkably, the morphology of the resulting structures could be finely tuned by adjusting the composition of the ternary solution, enabling the formation of highly ordered and hierarchically organized nanofibers with PLLA, as well as short-range-ordered micro/nanodots arrays with PLGA.

Beyond the successful fabrication of these nanostructures, this work also explored, for the first time, the potential of ASB-SANS-generated PLGA nanostructures as drug delivery platforms. When loaded with thionine as a hydrophilic model drug for a preliminary assessment of the release characteristics of the PLGA nanostructures, the latter demonstrated a biphasic drug release profile characterized by a significantly reduced (almost 60% less than in PLLA) initial burst release compared to a plain, non-nanostructured film. This behaviour is attributed to the increased crystallinity and compactness of the ASB-SANS-derived nanostructures, which modulate the polymer's hydration and erosion dynamics. While the sustained release phase showed comparable kinetics to that of the film, the modulation of the burst phase is critical to minimizing premature drug release, enhancing the therapeutic safety and efficacy of the delivery system.

These results position the ASB-SANS method as a promising, low-cost, and scalable strategy for the development of polymeric coatings with tailored drug release kinetics. Its compatibility with commonly used large-area substrates and biocompatible polymers opens up new perspectives for the fabrication of implantable devices, surface coatings, or patch-based systems capable of delivering therapeutic agents in a temporally controlled and spatially localized manner.

Author contributions

AFM: conceptualization, methodology, validation, formal analysis, investigation, resources, data curation, visualization, supervision, writing – review & editing. GS: writing – original draft, validation, formal analysis, resources, data curation, visualization, writing – review & editing. EBG: methodology, formal analysis, investigation, visualization, writing – review & editing. FM, SM, SP: formal analysis, writing – review & editing.

Conflicts of interest

There are no conflicts of interest to declare.

Data availability

The authors confirm that the data supporting the findings of this study are available within the article.

References

1 M. Zakaria, M. A. R. Bhuiyan, M. S. Hossain, N. M.-M. U. Khan, M. A. Salam and K. Nakane, Advances of polyolefins from fiber to nanofiber: fabrication and recent applications, *Discover Nano*, 2024, **19**, 24, DOI: 10.1186/s11671-023-03945-y.

2 X. Duan, H. I. Chen and C. Guo, Polymeric Nanofibers for Drug Delivery Applications: A Recent Review, *J. Mater. Sci.: Mater. Med.*, 2022, **33**, 78, DOI: 10.1007/s10856-022-06700-4.

3 P. Phutane, D. Telange, S. Agrawal, M. Gunde, K. Kotkar and A. Pethe, Biofunctionalization and Applications of Polymeric Nanofibers in Tissue Engineering and Regenerative Medicine, *Polymers*, 2023, **15**, 1202, DOI: 10.3390/polym15051202.

4 S. Shi, W. Bai, X. Chen, Y. Si, C. Zhi, H. Wu, Y. Su, W. Cai, B. Fei, C.-W. Kan, J. Hu and X. Wang, Advances in Nanofiber Filtration Membranes: From Principles to Intelligent Applications, *Adv. Funct. Mater.*, 2025, 2423284, DOI: 10.1002/adfm.202423284.

5 F. Boll, M. Fadda, M. Happel, M. Crisci, A. Athanassiou, B. Smarsly, F. Bella, F. Lamberti, G. Perotto and T. Gatti, Multicomponent Synergistic Contribution in Nanoengineered Nanofibers for Flexible Energy Storage, *ACS Appl. Energy Mater.*, 2024, **7**, 4733–4744, DOI: 10.1021/acsaem.4c00417.

6 J. Chen, Y. Fan, G. Dong, H. Zhou, R. Du, X. Tang, Y. Ying and J. Li, Designing biomimetic scaffolds for skin tissue engineering, *Biomater. Sci.*, 2023, **11**, 3051–3076, DOI: 10.1039/d3bm00046j.

7 T. Huang, Y. Zeng, C. Li, Z. Zhou, J. Xu, L. Wang, D.-G. Yu and K. Wang, Application and Development of Electrospun Nanofiber Scaffolds for Bone Tissue Engineering, *ACS Biomater. Sci. Eng.*, 2024, **10**, 4114–4144, DOI: 10.1021/acsbiomaterials.4c00028.

8 Z. Ma, W. Jia, J. Zhang, X. He, S. Liu, M. E. Hilal, X. Zhou, Z. Yang, Z. Chen, P. Shi and B. L. Khoo, Integrated Piezoelectric Vascular Graft for Continuous Real-Time Hemodynamics Monitoring, *Adv. Funct. Mater.*, 2024, **34**, 2409874, DOI: 10.1002/adfm.202409874.

9 S. Shi, X. Ou and D. Cheng, How Advancing is Peripheral Nerve Regeneration Using Nanofiber Scaffolds? A Comprehensive Review of the Literature, *Int. J. Nanomedicine*, 2023, **18**, 6763–6779, DOI: 10.2147/ijn.s436871.

10 P. Phutane, D. Telange, S. Agrawal, M. Gunde, K. Kotkar and A. Pethe, Biofunctionalization and Applications of Polymeric Nanofibers in Tissue Engineering and Regenerative Medicine, *Polymers*, 2023, **15**, 1202, DOI: 10.3390/polym15051202.

11 Y. Wang, D.-G. Yu, Y. Liu and Y.-N. Liu, Progress of Electrospun Nanofibrous Carriers for Modifications to Drug Release Profiles, *J. Funct. Biomater.*, 2022, **13**, 289, DOI: 10.3390/jfb13040289.

12 P. Huo, X. Han, W. Zhang, J. Zhang, P. Kumar and B. Liu, Electrospun Nanofibers of Polycaprolactone/Collagen as a Sustained-Release Drug Delivery System for Artemisinin, *Pharmaceutics*, 2021, **13**, 1228, DOI: 10.3390/pharmaceutics13081228.

13 A. M. Agiba, N. Elsayyad, H. N. ElShagea, M. A. Metwalli, A. O. Mahmoudsalehi, S. Beigi-Boroujeni, O. Lozano, A. Aguirre-Soto, J. L. Arreola-Ramirez, P. Segura-Medina and R. R. Hamed, Advances in Light-Responsive Smart Multifunctional Nanofibers: Implications for Targeted Drug Delivery and Cancer Therapy, *Pharmaceutics*, 2024, **16**, 1017, DOI: 10.3390/pharmaceutics16081017.

14 B. Abadi, N. Goshtasbi, S. Bolourian, J. Tahsili, M. Adeli-Sardou and H. Forootanfar, Electrospun hybrid nanofibers: Fabrication, characterization, and biomedical applications, *Front. Bioeng. Biotechnol.*, 2022, **10**, 986975, DOI: 10.3389/fbioe.2022.986975.

15 B. Singh, K. Kim and M.-H. Park, On-Demand Drug Delivery Systems Using Nanofibers, *Nanomaterials*, 2021, **11**, 3411, DOI: 10.3390/nano11123411.

16 X. Duan, H.-l. Chen and C. Guo, Polymeric Nanofibers for Drug Delivery Applications: A Recent Review, *J. Mater. Sci.:Mater. Med.*, 2022, **33**, 78, DOI: 10.1007/s10856-022-06700-4.

17 S. Farhaj, B. R. Conway and M. U. Ghori, Nanofibres in Drug Delivery Applications, *Fibers*, 2023, **11**, 21, DOI: 10.3390/fib11020021.

18 M. K. Gaydhane, C. S. Sharma and S. Majumdar, Electrospun nanofibres in drug delivery: advances in controlled release strategies, *RSC Adv.*, 2023, **13**, 7312–7328, DOI: 10.1039/d2ra06023j.

19 C. Feng, Y. Wang, J. Xu, Y. Zheng, W. Zhou, Y. Wang and C. Luo, Precisely Tailoring Molecular Structure of Doxorubicin Prodrugs to Enable Stable Nanoassembly, Rapid Activation, and Potent Antitumor Effect, *Pharmaceutics*, 2024, **16**, 1582, DOI: 10.3390/pharmaceutics16121582.

20 L. Zhong, Q. Zhu, X. Wang, G. Huang, J. Liu, H. Liu and Q. Wang, When nanocellulose meets liquid metal: a review of the synergistic frontier for flexible electronics, *Cellulose*, 2025, **32**, 9787–9818, DOI: 10.1007/s10570-025-06808-0.

21 Q. Wang, L. Zhong, Y. Zhou, G. Huang, J. Liu, H. Liu and Q. Zhu, Hierarchical cellulose nanopaper origami electronics, *Carbohydr. Polym.*, 2026, **373**, 124627, DOI: 10.1016/j.carbpol.2025.124627.

22 Z. Zheng, R. Wu, Q. Li, X. Wu, D. Qiu, Z. Wang and H. Liu, Water-resistant, flexible and transparent cellulose nanofibril film for exceptional oxygen-barrier performance under high humidity, *Carbohydr. Polym.*, 2026, **378**, 124966, DOI: 10.1016/j.carbpol.2026.124966.

23 R. Sun, Y. Chen, Y. Pei, W. Wang, Z. Zhu, Z. Zheng, L. Yang and L. Sun, The drug release of PLGA-based nanoparticles and their application in treatment of gastrointestinal cancers, *Heliyon*, 2024, **10**, e38165, DOI: 10.1016/j.heliyon.2024.e38165.

24 A. Ershad-Langroudi, N. Babazadeh, F. Alizadegan, S. M. Mousaei and G. Moradi, Polymers for implantable devices, *J. Ind. Eng. Chem.*, 2024, **137**, 61–86, DOI: 10.1016/j.jiec.2024.03.030.

25 Z. Li, N. Bhaskar, G. Erel-Akbaba, Y. Zhu, G. Ge, J. Park, K. Angadi, A. Duhoon and T. D. Nguyen, Current advances of biodegradable and biocompatible nanofiber-based materials for tissue engineering and drug delivery, *MRS Commun.*, 2025, **5**, 374–390, DOI: 10.1557/s43579-025-00728-7.

26 J. Yang, H. Zeng, Y. Luo, Y. Chen, M. Wang, C. Wu and P. Hu, Recent Applications of PLGA in Drug Delivery Systems, *Polymers*, 2024, **16**, 2606, DOI: 10.3390/polym16182606.

27 M. S. Razavi, A. Abdollahi, A. Malek-Khatabi, N. M. Ejarestaghi, A. Atashi, N. Yousefi, P. Ebrahimnejad, M. A. Elsawy and R. Dinarvand, Recent advances in PLGA-based nanofibers as anticancer drug delivery systems, *J. Drug Delivery Sci. Technol.*, 2023, **85**, 104587, DOI: 10.1016/j.jddst.2023.104587.

28 L. S. Dolci, R. C. Perone, R. Di Gesù, M. Kurakula, C. Gualandi, E. Zironi, T. Gazzotti, M. T. Tondo, G. Pagliuca, N. Gostynska, V. A. Baldassarro, M. Cescatti, L. Giardino, M. L. Focarete, L. Calzà, N. Passerini and M. L. Bolognesi, Design and *In Vitro* Study of a Dual Drug-Loaded Delivery System Produced by Electrospinning for the Treatment of Acute Injuries of the Central Nervous System, *Pharmaceutics*, 2021, **13**, 848, DOI: 10.3390/pharmaceutics13060848.

29 Y. Sun, J. Heacock, J. Liu and Y. V. Li, Enhanced Fibrous Scaffolds for Drug Delivery Applications: Core–Shell Fiber Scaffolds with Antibiotic-Encapsulated Poly(lactic-co-glycolic acid) Nanoparticles, *ACS Appl. Nano Mater.*, 2025, **8**, 5853–5861, DOI: 10.1021/acsanm.5c00972.

30 M. A. Téllez Corral, J. C. Villamil Poveda, N. S. Roa Molina, L. Otero, Z. J. Rivera Monroy, J. G. Castañeda, C. M. Parra Giraldo and M. E. Cortés, In-vitro antibiofilm activity of polycaprolactone- poly (lactic-co-glycolic acid) nanofibers loaded amphotericin B, antimicrobial peptide LfcinB (21–25)Pal and zinc oxide for local treatment of periodontitis associated with obstructive sleep apnea, *J. Drug Delivery Sci. Technol.*, 2024, **94**, 105522, DOI: 10.1016/j.jddst.2024.105522.

31 Y. Cho, J. W. Beak, M. Sagong, S. Ahn, J. S. Nam and I.-D. Kim, Electrospinning and Nanofiber Technology: Fundamentals, Innovations, and Applications, *Adv. Mater.*, 2025, e2500162, DOI: 10.1002/adma.202500162.

32 Y. Chen, X. Dong, M. Shafiq, G. Myles, N. Radacsi and X. Mo, *Adv. Fiber Mater.*, 2022, **4**, 959–986, DOI: 10.1007/s42765-022-00170-7.

33 T. S. Gilmore and P.-I. Gouma, Scalable electrospinning using a desktop, high throughput, self-contained system, *Sci. Rep.*, 2024, **14**, 25844, DOI: 10.1038/s41598-024-76766-3.

34 L. Maduna and A. Patnaik, Challenges Associated with the Production of Nanofibers, *Processes*, 2024, **12**, 2100, DOI: 10.3390/pr12102100.

35 A. Fraleoni-Morgera, Fast Fabrication of Large-Area, Nanostructured Arrays from Polymers or Carbon Nanotubes by Wet-Processing, *Small*, 2011, **7**, 321–325, DOI: 10.1002/smll.201001281.

36 I. H. Eryilmaz, J. Mohanraj, S. Dal Zilio and A. Fraleoni-Morgera, Controlled self-organization of polymer nanopatterns over large areas, *Sci. Rep.*, 2017, **7**, 10526, DOI: 10.1038/s41598-017-09463-z.

37 J. Mohanraj, L. Puzzi, E. Capria, S. Corvaglia, L. Casalis, L. Mestroni, O. Sbaizero and A. Fraleoni-Morgera, Easy fabrication of aligned PLLA nanofibers-based 2D scaffolds suitable for cell contact guidance studies, *Mater. Sci. Eng., C*, 2016, **62**, 301–306, DOI: 10.1016/j.msec.2015.12.042.

38 E. Betz-Güttner, M. Righi, S. Micera and A. Fraleoni-Morgera, Directional Growth of cm-Long PLGA Nanofibers by a Simple and Fast Wet-Processing Method, *Materials*, 2022, **15**, 687, DOI: 10.3390/ma15020687.

39 C. Bertoni, P. Naclerio, E. Viviani, S. Dal Zilio, S. Carrato and A. Fraleoni-Morgera, Nanostructured P3HT as a Promising Sensing Element for Real-Time, Dynamic Detection of Gaseous Acetone, *Sensors*, 2019, **19**, 1296, DOI: 10.3390/s19061296.

40 A. Fraleoni-Morgera, G. Palma and J. R. Plaisier, Fast fabrication over large areas of P3HT nanostructures with high supramolecular order, *RSC Adv.*, 2013, **3**, 15664–15669, DOI: 10.1039/c3ra41612g.

41 E. Rabinowitch and L. F. Epstein, Polymerization of Dyestuffs in Solution. Thionine and Methylene Blue, *J. Am. Chem. Soc.*, 1941, **63**, 69–78, DOI: 10.1021/ja01846a011.

42 T. M. Birshtein and V. A. Pryamitsyn, Coil-Globule Type Transitions in Polymers. 2. Theory of Coil-Globule Transition in Linear Macromolecules, *Macromolecules*, 1991, **24**, 1554–1560, DOI: 10.1021/ma00007a017.

43 I. Nishio, S.-T. Sun, G. Swislow and T. Tanaka, First observation of the coil–globule transition in a single polymer chain, *Nature*, 1979, **281**, 208–209, DOI: 10.1038/281208a0.

44 S. Cattarinussi and G. Jug, Coil-globule transition temperature enhancement in a polymer molecule adsorbed to a wall, *J. Phys. A: Math. Gen.*, 1990, **23**, 2701–2706, DOI: 10.1088/0305-4470/23/12/043.

45 S. Venkatram, C. Kim, A. Chandrasekaran and R. Ramprasad, Critical Assessment of the Hildebrand and Hansen Solubility Parameters for Polymers, *J. Chem. Inf. Model.*, 2019, **59**(10), 4188–4194, DOI: 10.1021/acs.jcim.9b00656.

46 C. M. Hansen, *Hansen Solubility Parameters – A User's Handbook*, Boca Raton, CRC press, 2nd edn, 2007, DOI: 10.1201/9781420006834.

47 S. J. Abbott, https://www.stevenabbott.co.uk/practical-solubility/hsp-basics.php, data collected in March 2026.

48 S. J. Abbott, Chemical Compatibility of Poly(Lactic Acid): A Practical Framework Using Hansen Solubility Parameters, in *Poly(lactic Acid): Synthesis, Structures, Properties, Processing, and Applications*, Wiley, 2010, pp. 83–93, DOI: 10.1002/9780470649848.ch7.

49 M. Esmaeili, G. Pircheraghi, R. Bagheri and V. Altstädt, Poly(lactic acid)/coplasticized thermoplastic starch blend: Effect of plasticizer migration on rheological and

mechanical properties, *Polym. Adv. Technol.*, 2018, 1–13, DOI: 10.1002/pat.4517.

50 S. Schenderlein, M. Lück and B. W. Müller, Partial solubility parameters of poly(d,l-lactide-co-glycolide), *Int. J. Pharm.*, 2004, **286**, 19–26, DOI: 10.1016/j.ijpharm.2004.07.034.

51 N. Goonoo, A. Bhaw-Luximon and D. Jhurry, Drug Loading and Release from Electrospun Biodegradable Nanofibers, *J. Biomed. Nanotechnol.*, 2014, **10**, 2173–2199, DOI: 10.1166/jbn.2014.1885.

52 L. Weng and J. Xie, Smart Electrospun Nanofibers for Controlled Drug Release: Recent Advances and New Perspectives, *Curr. Pharm. Des.*, 2015, **21**, 1944–1959, DOI: 10.2174/1381612821666150302151959.

53 T. Amna, M. S. Hassan, F. N. Gharsan, S. Rehman and F. A. Sheikh, Nanotechnology in Drug Delivery Systems: Ways to Boost Bioavailability of Drugs, in *Nanotechnology for Infectious Diseases*, ed. S. Hameed and S. Rehman, Springer, Singapore, 2022, DOI: 10.1007/978-981-16-9190-4_10.

54 H. Maleki, M. Doostan, S. Shojaei, M. Doostan, H. Stamatis, E. Gkantzou, A. Bonkdar and K. Khoshnevisan, Nanofiber-based systems against skin cancers: therapeutic and protective approaches, *J. Drug Delivery Sci. Technol.*, 2023, **82**, 104367, DOI: 10.1016/j.jddst.2023.104367.

55 M. Redrado, Z. Xiao, K. Upitak, B.-T. Doan, C. M. Thomas and G. Gasse, Applications of Biodegradable Polymers in the Encapsulation of Anticancer Metal Complexes, *Adv. Funct. Mater.*, 2024, **34**, 2401950, DOI: 10.1002/adfm.202401950.

56 D. R. Perinelli, M. Cespi, G. Bonacucina and G. F. Palmieri, PEGylated polylactide (PLA) and poly(lactic-*co*-glycolic acid) (PLGA) copolymers for the design of drug delivery systems, *J. Pharm. Invest.*, 2019, **49**, 443–458, DOI: 10.1007/s40005-019-00442-2.

57 A. Al-Abduljabbar and I. Farooq, Electrospun Polymer Nanofibers: Processing, Properties, and Applications, *Polymers*, 2023, **15**, 65, DOI: 10.3390/polym15010065.

58 R. Abdulhussain, A. Adebisi, B. R. Conway and K. Asare-Addo, Electrospun nanofibers: Exploring process parameters, polymer selection, and recent applications in pharmaceuticals and drug delivery, *J. Drug Delivery Sci. Technol.*, 2023, **90**, 105156, DOI: 10.1016/j.jddst.2023.105156.

59 A. Nadaf, A. Gupta, N. Hasan, Fauziya, S. Ahmad, P. Kesharwani and F. J. Ahmad, Recent update on electrospinning and electrospun nanofibers: current trends and their applications, *RSC Adv.*, 2022, **12**, 23808–23828, DOI: 10.1039/d2ra02864f.

60 M. A. Bonakdar and D. Rodrigue, Electrospinning: Processes, Structures, and Materials, *Macromol*, 2024, **4**, 58–103, DOI: 10.3390/macromol4010004.

61 Y. Lu, D. Cheng, B. Niu, X. Wang, X. Wu and A. Wang, Properties of Poly (Lactic-co-Glycolic Acid) and Progress of Poly(Lactic-co-Glycolic Acid)-Based Biodegradable Materials in Biomedical Research, *Pharmaceuticals*, 2023, **16**, 454, DOI: 10.3390/ph16030454.

62 J. Tolivia, D. Tolivia and A. Navarro, Differential thionin block staining of nerve cells and fibers for paraffin-embedded material in mammalian central nervous system, *Neurosci. Lett.*, 1989, **102**, 155–158, DOI: 10.1016/0304-3940(89)90071-2.

63 P. Derkx and D. H. Birkenhäger-Frenkel, A thionin stain for visualizing bone cells, mineralizing fronts and cement lines in undecalcified bone sections, *Biotech. Histochem.*, 1995, **70**, 70–74, DOI: 10.3109/10520299509108320.

64 S. J. Cloete, A. Petzer and J. P. Petzer, Interactions of dye compounds that are structurally related to methylene blue with acetylcholinesterase and butyrylcholinesterase, *Chem. Biol. Drug Des.*, 2021, **97**, 854–864, DOI: 10.1111/cbdd.13814.

65 V. E. Nicotra, M. F. Mora, R. A. Iglesias and A. M. Baruzzi, Spectroscopic characterization of thionine species in different media, *Dyes Pigm.*, 2008, **76**, 315–318, DOI: 10.1016/j.dyepig.2006.08.012.

66 R. D. Deegan, O. Bakajin, T. F. Dupont, G. Huber, S. R. Nagel and T. A. Witten, Capillary flow as the cause of ring stains from dried liquid drops, *Nature*, 1997, **389**, 827–829, DOI: 10.1038/39827.

67 S. Moffa, S. Carradori, F. Melfi, A. Fontana, M. Ciulla, P. Di Profio, M. Aschi, R. D. Wolicki, S. Pilato and G. Siani, Fine-tuning of membrane permeability by reversible photoisomerization of aryl-azo derivatives of thymol embedded in lipid nanoparticles, *Colloids Surf., B*, 2024, **241**, 114043, DOI: 10.1016/j.colsurfb.2024.114043.

68 S. Moffa, M. Aschi, M. Bazzoni, F. Cester Bonati, A. Secchi, P. Bruni, P. Di Profio, A. Fontana, S. Pilato and G. Siani, Synthesis, characterization, and computational study of aggregates from amphiphilic calix[6]arenes. Effect of encapsulation on degradation kinetics of curcumin, *J. Mol. Liq.*, 2022, **368**, 120731, DOI: 10.1016/j.molliq.2022.120731.

69 J. Yoo and Y.-Y. Won, Phenomenology of the Initial Burst Release of Drugs from PLGA Microparticles, *ACS Biomater. Sci. Eng.*, 2020, **6**, 6053–6062, DOI: 10.1021/acsbiomaterials.0c01228.

70 S. Bhattacharjee, Understanding the burst release phenomenon: toward designing effective nanoparticulate drug-delivery systems, *Ther. Delivery*, 2021, **12**, 21–36, DOI: 10.4155/tde-2020-0099.

71 J. P. K. Tan, Q. Wang and K. C. Tam, Control of burst release from nanogels *via* layer by layer assembly, *J. Controlled Release*, 2008, **128**, 248–254, DOI: 10.1016/j.jconrel.2008.03.012.